FDTD Analysis of ELF Wave Propagation in Inhomogeneous Subionospheric Waveguide Models

Hayakawa, M. and T. Otsuyama
Department of Electronic Engineering, The University of Electro-Communications, 1-5-1 Chofugaoka, Chofu, Tokyo 182-8585, Japan
Tel: +81 424 43 5159, Fax: +81 424 43 5168, E-mail hayakawa@whistler.ee.uec.ac.jp

ABSTRACT. The space formed by the ground and ionosphere is known to act as a resonator for extremely low frequency (ELF) waves. Lightning discharges trigger this global resonance, which is known as Schumann resonances at the frequencies of 8, 14, 21Hz etc. Even though the inhomogeneity (like day-night asymmetry, local perturbation etc.) is important for such subionospheric ELF propagation, the previous analyses have been always made by some approximations because the problem is too complicated to be analyzed by exact full-wave analysis. This paper presents the first application of the conventional FDTD method to such subionospheric ELF wave propagation, in which any kinds of inhomogeneities can be included in the analysis, to be compared with the observational results. We show the application of FDTD to our problem and present a few numerical computational results to be compared with those by the pre-existing analysis method.

1. Introduction

Recently there has been again a great interest in subionospheric ELF waves because of the two important findings. The first one is the suggestion by Williams [1] that the global warming which is a very important issue for human being, can be effectively monitored by the intensity of Schumann resonances. Schumann resonance is a global resonance phenomenon in the Earth-ionosphere cavity as shown in Fig. 1, which is triggered by lightning discharges in the thunder-active equatorial region. The resonance frequencies are 8, 14, 21Hz etc. in the ELF range. The second reason is closely associated with the finding of optical phenomena (red sprites etc.) in the mesosphere and the lower ionosphere, and it is found that this mesospheric optical phenomenon is a source of strong ELF signals (called ELF transients) [2]. This ELF transient signal is one of the important tools for the study of those mesospheric optical phenomena and then the electrodynamic coupling between the atmosphere and ionosphere.

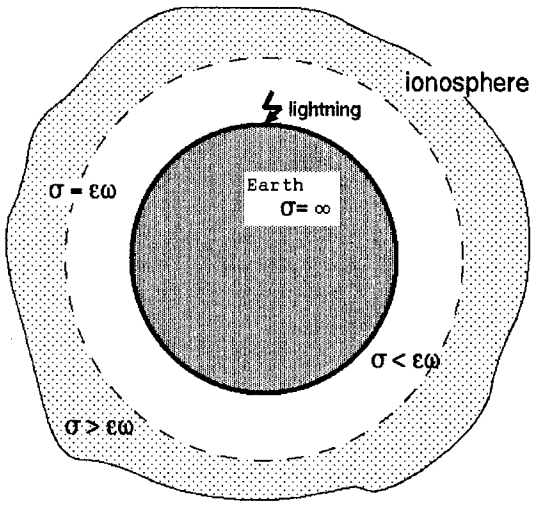

Fig. 1. Configuration of the Earth-ionosphere cavity.

There have been published a few monographs dealing with the subionospheric ELF propagation [3-5]. Schumann [6] was the first to predict the presence of resonances in the spherical earth-ionosphere cavity and suggested a mathematical formulation of the propagation problem at ELF. A great simplification is the presence of only a single globally propagating, zero-order TEM mode [7], while all the higher-order modes attenuate severely at distances of several waveguide effective heights. Despite this simplification, the complex structure of the lower ionosphere imposes an intricate three-dimensional electrodynamical problem that cannot be reduced to practical techniques without certain additional simplifying assumptions. This is the reason why several fundamental observed properties of Schumann resonances cannot be well explained [5,8], and please look at the forthcoming monograph on ELF [8] indicating a lot of unsolved problems in the ELF range. The factors of making the problem very complete are (1) radially (vertically) inhomogeneity of the ionosphere, (2) day-night asymmetry, (3) local ionospheric perturbations etc.

In this sense it is highly required that very complicated situations should be solved in an exact way even by using the numerical methods. If the exact numerical solutions are available for any complicated cavity, it would be possible for us to examine the validity of the previous approximate solutions.

2. Three-dimensional FDTD analysis

The above discussion has led to the requirement for a three-dimensional finite-difference time domain (FDTD) application to our ELF propagation problem in spherical coodinates with azimuthal dependence. Fortunately, this 3D FDTD code has been developed by Holland [9], which can be used in our application. Fig. 2 (right panel) shows the spherical coordinate system (r, θ, ϕ) and location of a unit cell. The left panel of Fig. 2 illustrates the location of field-evaluation points on a unit cell. As shown in Fig. 2, we build a cell entitled I, J and K along each of three axes (r, θ, and ϕ) . In the r direction I = 1 is the starting grid (r = a (Earth's radius) 6.4Mm) and this ground is assumed to be a perfect conductor. I = N_r is the outermost radial boundary, is taken to be r = a + 150 km and to be a perfect conductor. In the θ direction J = 1 is the North Pole (θ = 0°) and J = N_θ is the South Pole (θ = 180°) . The coordinate ϕ indicates the longitude in such a way that K = 1 and K = N_ϕ are the same point, but the latter has encircled the globe. On this condition the six electromagnetic field components are expressed by Holland [9].

The Maxwell's equations to be solved are expressed as follows [10].

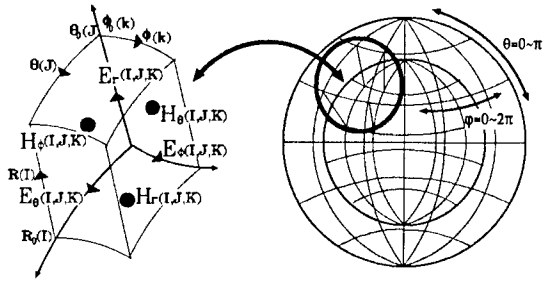

Fig. 2. The spherical coordinate system (r, θ, ϕ) and location of a unit cell (right panel). The left panel illustrates the location of field-evaluation points on the unit cell.

$$\begin{cases} \nabla \times \mathbf{E} = -\mu_0 \dfrac{\partial \mathbf{H}}{\partial t} \\ \nabla \times \mathbf{H} = \varepsilon_0 \dfrac{\partial \mathbf{E}}{\partial t} + \sigma \mathbf{E} + \mathbf{J}_{ext} \end{cases} \tag{1}$$

where **E** is the electric field, **H** is the magnetic field, ε_0, μ_0 are the dielectric constant and permeability of free space, σ is the conductivity which is a function of space, and $\mathbf{J}_{ext}$ is the current source of the system (here this is a lightning discharge). Here we write down the field updating equations in the spherical coordinates as follows.

In the region of I=1~N_{r-1}, J=2~$N_{\theta-1}$ and K=2~N_ϕ, the field updating equation for E_r component is given by;

$$\begin{aligned} E_r(\mathrm{I,J,K})^{n+1/2} = {} & \frac{\varepsilon_0/\Delta t - \sigma/2}{\varepsilon_0/\Delta t + \sigma/2} E_r(\mathrm{I,J,K})^{n-1/2} + (\varepsilon_0/\Delta t + \sigma/2)^2 \\ & \cdot \left(\frac{1}{R(\mathrm{I}) \sin\theta_0(\mathrm{J})} \cdot \left[\frac{\sin\theta(\mathrm{J}) H_\phi(\mathrm{I,J,K})^n - \sin\theta(\mathrm{J}-1) H_\phi(\mathrm{I,J-1,K})^n}{\Delta\theta} \right. \right. \\ & \left. \left. - \frac{H_\theta(\mathrm{I,J,K})^n - H_\theta(\mathrm{I,J,K-1})^n}{\Delta\phi} \right] \right) \end{aligned} \tag{2}$$

The corresponding equation for E_θ is as follows.

$$\begin{aligned} E_\theta(\mathrm{I,J,K})^{n+1/2} = {} & \frac{\varepsilon_0/\Delta t - \sigma/2}{\varepsilon_0/\Delta t + \sigma/2} E_\theta(\mathrm{I,J,K})^{n-1/2} + (\varepsilon_0/\Delta t + \sigma/2)^2 \\ & \cdot \left(\frac{1}{R_0(\mathrm{I})} \cdot \left[\frac{H_r(\mathrm{I,J,K})^n - H_r(\mathrm{I,J,K-1})^n}{\sin\theta(J)\Delta\phi} \right. \right. \\ & \left. \left. - \frac{R(\mathrm{I}) H_\phi(\mathrm{I,J,K})^n - R(\mathrm{I}-1) H_\phi(\mathrm{I}-1,\mathrm{J,K})^n}{\Delta r} \right] \right) \end{aligned} \tag{3}$$

and this equation pertains to I=1~N_{r-1}, J=2~$N_{\theta-1}$ and K=2~N_ϕ. And then, the field updating equation for E_ϕ component is as follows.

$$E_\phi(\mathrm{I,J,K})^{n+1/2} = \frac{\varepsilon_0/\Delta t - \sigma/2}{\varepsilon_0/\Delta t + \sigma/2} E_\phi(\mathrm{I,J,K})^{n-1/2} + (\varepsilon_0/\Delta t + \sigma/2)^2 \cdot \left(\frac{1}{R_0(\mathrm{I})} \left[\frac{R(I) H_\theta(\mathrm{I,J,K})^n - R(\mathrm{I}-1) H_\theta(\mathrm{I}-1,\mathrm{J,K})^n}{\Delta r} - \frac{H_r(\mathrm{I,J,K})^n - H_r(\mathrm{I,J}-1,\mathrm{K})^n}{\Delta\theta} \right] \right) \tag{4}$$

for I=2~N_r, J=1~$N_{\theta-1}$ and K=2~N_ϕ. Δr, $\Delta\theta$ and $\Delta\phi$ are the grid size in the r, θ, ϕ directions, and Δt is time step.

The field updating equation for magnetic field components (H_r, H_θ, H_ϕ) are given as follows.

$$H_r(\mathrm{I,J,K})^{n+1} = H_r(\mathrm{I,J,K})^n - \frac{\Delta t}{\mu_0} \left(\frac{1}{R_0(\mathrm{I})\sin\theta(\mathrm{J})} \left[\frac{\sin\theta_0(\mathrm{J}+1) E_\phi(\mathrm{I,J}+1,\mathrm{K})^{n+1/2} - \sin\theta_0(\mathrm{J}) E_\phi(\mathrm{I,J,K})^{n+1/2}}{\Delta\theta} - \frac{E_\theta(\mathrm{I,J,K}+1)^{n+1/2} - E_\theta(\mathrm{I,J,K})^{n+1/2}}{\Delta\phi} \right] \right) \tag{5}$$

for I=2~N_r, J=1~$N_{\theta-1}$ and K=1~$N_{\phi-1}$.

$$H_\theta(\mathrm{I,J,K})^{n+1} = H_\theta(\mathrm{I,J,K})^n - \frac{\Delta t}{\mu_0} \cdot \left(\frac{1}{R(\mathrm{I})} \left[\frac{E_r(\mathrm{I,J,K}+1)^{n+1/2} - E_r(\mathrm{I,J,K})^{n+1/2}}{\sin\theta_0(\mathrm{J})\Delta\phi} - \frac{R_0(\mathrm{I}+1) E_\phi(\mathrm{I}+1,\mathrm{J,K})^{n+1/2} - R_0(\mathrm{I}) E_\phi(\mathrm{I,J,K})^{n+1/2}}{\Delta r} \right] \right) \tag{6}$$

for I=1~N_{r-1}, J=2~$N_{\theta-1}$ and K=1~$N_{\phi-1}$.

$$H_\phi(\mathrm{I,J,K})^{n+1} = H_\phi(\mathrm{I,J,K})^n - \frac{\Delta t}{\mu_0} \cdot \left(\frac{1}{R(\mathrm{I})} \left[\frac{R(\mathrm{I}+1) E_\theta(\mathrm{I}+1,\mathrm{J,K})^{n+1/2} - R(\mathrm{I}) E_\theta(\mathrm{I,J,K})^{n+1/2}}{\Delta r} - \frac{E_r(\mathrm{I,J}+1,\mathrm{K})^{n+1/2} - E_r(\mathrm{I,J,K})^{n+1/2}}{\Delta\theta} \right] \right) \tag{7}$$

for I=1~N_{r-1}, J=1~$N_{\theta-1}$ and K=1~$N_{\phi-1}$.

The field components are on a modified Yee cell with unit vectors $\hat{r}$, $\hat{\theta}$, and $\hat{\varphi}$, and the corresponding indices I, J, K. Spatial locations are given in term of positions R_0(I), θ_0(J), ϕ_0(K). Points lying midway between these locations are given by R(I), θ(J), ϕ(K).

3. Modeling of conductivity profile and current source, and some numerical examples

In order to verify the usefulness of this 3D FDTD computation, we show some numerical results for a uniform cavity without any day-night asymmetry, because we can compare our own results with the previous analytical computations [11,12]. However, the height profile of the conductivity is definitely induced in our computations.

First we indicate the height profile of the atmospheric conductivity, which is expressed by,

$$\sigma(z) = \sigma_0 \exp(z/h) \tag{8}$$

where z is the height above the ground and h is the scale height (h = 6km). σ_0 is assumed to be

10^{-14}[S/m]. This is a typical profile [10]. Next we assume a lightning discharge current in the form of two exponentials by Bruce and Golde [13], but we adopt a model with much slower time variation than the actual lightning in order to validate the horizontal grid size of 250km.

$$I(t) = I_0\{\exp(-70t) - \exp(-100t)\} \qquad (9)$$

where t is in second. Assuming this current source, we made the FDTD computations in which the grid size in r is 2km, and the grid sizes in θ and ϕ are $\pi/72$ (about 250km).

Fig. 3 illustrates the computational results on the temporal evolution of horizontal magnetic field for four different distances (d = 5, 10, 15 and 20 Mm, indicating the distance in the θ direction) when the current source is located at the equator ($\theta=\pi/2$, ϕ = 0°). The pulse is generated at $t = 0$ and we can understand the propagation of a pulse in the V waveguide; we notice the direct wave and its corresponding antipodal wave. As you see from this figure, with the increase in propagation distance, the higher frequency components will decay so that we have a spread in waveform for larger propagation distances. The horizontal magnetic field of the antipodal wave is opposite in sign to that of the direct wave, so that the signal for d = 20Mm is zero because of the complete cancellation of the direct and antipodal waves. An important characteristic from this figure is that we expect severe damping between d = 5Mm and 10Mm, but negligible damping between d = 10Mm and 15Mm. These numerical computations are compared with the corresponding computation for their model [11] (the result is shown in Fig. 4), in which there exist some differences in the modeling. The first one is the difference in the input signal (source) because they used a delta function. The sign of the horizontal magnetic field is taken to

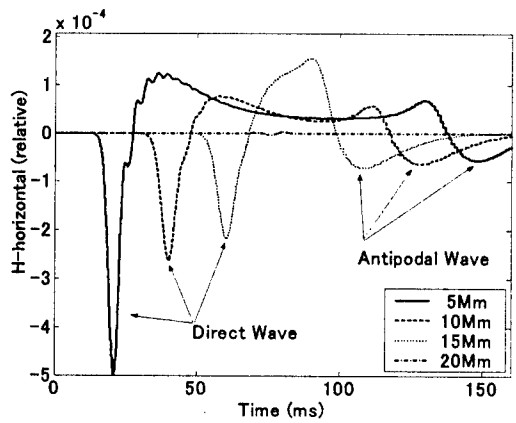

Fig. 4. Computational result of the temporal evolution of horizontal magnetic field for four different propagation distances (d=5, 10, 15 and 20 Mm).

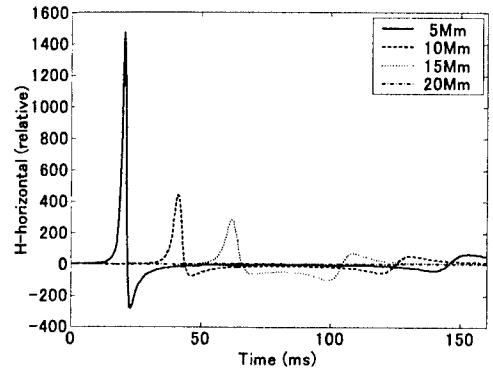

Fig. 3. Same as Fig. 3, but with the previous analytical method[11]. This figure should be compared with Fig. 3.

be oppose to that in this paper. We have found an extremely good similarity between these two figures, suggesting the usefulness of this 3D FDTD analysis in subionospheric ELF propagation. Another difference is definitely due to the difference in propagation constants. They [11] have used a heuristic propagation constant (v_1 and v_2) based on the experimental data,

$$v(f) = v_1 - iv_2 = (f-2)/6 - if/100, \qquad (10)$$

where f is frequency, and v_1, v_2 are real and imaginary part of propagation constant, respectively.

On the other hand, we have used the atmospheric conductivity profile, Eq.(8) as mentioned before. By using the approximate formulas by Greifinger and Greifinger [14], we can estimate the real and imaginary parts of the propagation constant for our ionospheric model. These results are shown in Fig. 5. Fig. 5(a) refers to the real part, while Fig. 5(b) refers to the imaginary part (or attenuation constant) of the propagation constant. The real parts are nearly identical for the two models, but we see a significant difference in the imaginary part (i.e. damping effect). Especially we notice a lot of difference in the attenuation constant at higher frequencies. In the paper [11], they used the heuristic propagation constant, Eq. (10), so that they have not indicated any explicit conductivity height profile. Of course it is theoretically possible for us to obtain the conductivity profile by some approximations from Eq. (10), but this kind of job is not so meaningful. In our next paper we will compare the attenuation from both methods under the same conductivity profile in order to prove the deviation in Fig. 5(b) is caused by different computational models instead of numerical errors.

Finally, we show the last figure for exact comparison between ours and the previous model [11] for the same propagation distance (d=10Mm) in Fig. 6.

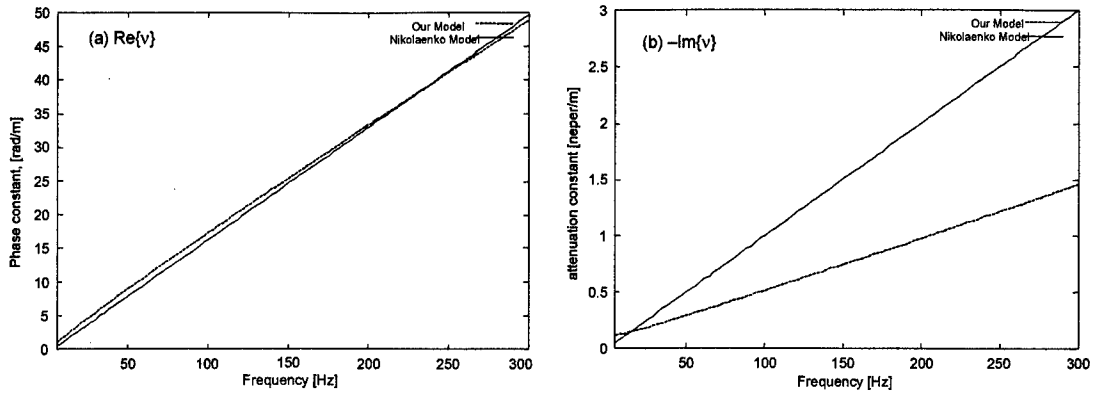

Fig. 5. Comparison of propagation constant. (a) refers to the propagation constant (real part), while (b) the imaginary part, indicating attenuation constant. Two models are compared; our model and Nickolaenko and Hayakawa [11]

4. Conclusions and future application of this FDTD analysis to much more complicated models

In the previous section we have shown only one example of our FDTD analysis for subionospheric ELF propagation and a comparison with the previous analytical solution has indicated that our FDTD application would be of great potential in our future studies. As you see from the above discussion, the field updating mechanism is exactly the same as that of the high-frequency FDTD [16], and it seems that there is no special treatment in the ELF wave analysis. We can list what we will be able to do in this ELF field by means of our FDTD analysis.

As for the ELF propagation itself (such as the propagation of ELF transients (Q bursts, slow tails)), we can study the reflection mechanism of these ELF waves in the lower ionosphere in details by comparing our FDTD results with the previously proposed approximations [14,15].

Then, as for Schumann resonance, there are

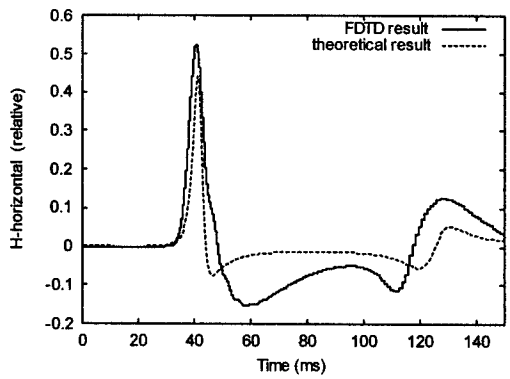

Fig. 6. Comparison of the ELF waveforms for a particular d=10Mm estimated by our method and previous method [11].

several possibilities of the application of our FDTD method. For example, (1) the full consideration of day-night asymmetry in order to well explain the diurnal variation of Schumann resonance intensity and frequencies, (2) the local perturbation (such as the perturbation at high latitudes (auroral regions)).

We will use our FDTD analysis for these above questions in order to improve the physics coming from these subionospheric ELF propagation studies.

REFERENCES

[1] E. R. Williams. The Schumann resonance: A global tropical thermometer. Science, 256, 1184-1187, 1992.

[2] D. J. Boccipio, E. R. Williams, S. J. Heckman, W. A. Lyons, I. T. Baker and R. Boldi. Sprites, ELF transients, and positive ground stroke. Science, 269, 1088-1091, 1995.

[3] J. R. Wait. *Electromagnetic Waves in Stratified Media. Perganion Press*, Oxford, 1962.

[4] J. Galejs. *Terrestrial Propagation of Long Electromagnetic Waves*. Pergamon Press, Oxford, 1972.

[5] P. V. Bliok, A. P. Nikolaenko and Yu. F. Filippov, *Schumann Resonances in the Earth-Ionosphere Cavity*, Peter Pergrinus Ltd., 1980.

[6] W. O. Schumann. On the radiation free self-oscillations of a conducting sphere, which is surrounded by an air layer and an ionospheric shell [in German]. Zeitschrift fur Naturforschung, 7, 149-154, 1952.

[7] T. Madden and W. Thompson. Low frequency electromagnetic oscillations of Earth-ionosphere cavity. Rev. Geophys., 3, 211-254, 1965.

[8] A. P. Nickolaenko and M. Hayakawa, *Resonances in the Earth-Ionosphere Cavity*, Kluwer Academic Publishers, Dordrecht, 2002.

[9] R. Holland. THREDS: A finite-difference time-domain EMP code in 3D spherical coordinates.

IEEE Trans. Nuclear Science, NS-30(6), 4592-4595, 1983.

[10] D. D. Sentman. Schumann resonances. In Handbook of Atmospheric Electrodynamics, Ed. by H. Volland, vol. 1, 267-310, CRC Press, 1995.

[11] A. P. Nickolaenko and M. Hayakawa. Natural electromagnetic pulses in the ELF range. Geophys. Res. Lett., 25(16), 3103-3106, 1998.

[12] A. P. Nickolaenko, M. Hayakawa, I. G. Kudintseva, S. V. Myand and L. M. Rabinowicz. ELF sub-ionospheric pulse in time domain, Geophys. Res. Lett., 26(7), 999-1002, 1999.

[13] C. E. R. Bruce and R. H. Golde. The lightning discharge. J. Inst. Electr. Eng., 88, 487, 1941.

[14] C. Greifinger and P. Greifinger. Approximate method for determining ELF eigenvalues in the earth-ionosphere waveguide. Radio Science, 13, 831, 1978.

[15] V. C. Mushtak and E. R. Williams. ELF propagation parameters for uniform models of the Earth-ionosphere waveguide. J. Atmos. Soler-terr. Phys., 18, 1989-2001, 2002.

[16] K.Kunz and R.J. Luebbers. *The Finite Difference Time Domain Method for Electromagnetics*, CRC Press, Boca Raton, USA, 1993.

Masashi Hayakawa obtained Bachelor degree, Master degree from Nagoya University in 1966 and 1968, respectively. Doctor of Engineering from the same university in 1974. In 1970 he joined Research Institute of Atmospherics of Nagoya University as a Research Associate, and become Assistant and Associate Professors there. Since 1991 he has been a professor of the University of Electro-Communications and has been working on space physics, atmospheric electricity, seismo-electromagnetics, EMC, inversion problem. He was URSI Commission E chair (1996-1999), and he is now co-editor of Radio Science. IEICE, AGU, URSI member.

Takuya Otsuyama obtained Bachelor degree, Master degree from University of Electro-Communications in 1996 and 1998, respectively. And he obtained Doctor of Engineering from the same university in 2002. He has been working on upper atmosphere discharge and Trimpi phenomena. He joined Sankosha Co. and is working on lightning detection and application.